Activation characteristic of a vibro-impact energy sink and its application to chatter control in turning

Tao Li, Donghai Qiu, Sébastien Seguy, Alain Berlioz

Activation characteristic of a vibro-impact energy sink and its application to chatter control in turning

T. Li*, D. Qiu, S. Seguy, A. Berlioz

Institut Clément Ader (ICA), CNRS-INSA-ISAE-Mines Albi-UPS, Université de Toulouse, 3 rue Caroline Aigle, 31400, Toulouse, France

Abstract

The ultimate goal of this paper is to propose a procedure for the optimal design of a Vibro-Impact (VI) Nonlinear Energy Sink (NES) to control the vibration of any possible linear or nonlinear main systems. To this end, the activation characteristic of VI NES at a range of displacement amplitude of a main system is generalized from linear systems to nonlinear systems. It is theoretically proved and experimentally observed that this activation characteristic is almost independent of frequency, which provides direct proof for the effectiveness of VI NES in a broad frequency bandwidth. In terms of vibration control, this feature is very attractive and builds a bridge between linear and nonlinear systems. Then it is applied for the design of VI NES attached to nonlinear systems. In this way, the design of VI NES for a nonlinear system is simplified to the optimal design for a linear system, which is designed to be similar to this target nonlinear system. Because the latter can be analytically calculated, the proposed method is feasible from a quantitative perspective. Finally, this activation characteristic and a proposed design method are applied to control chatter in a turning process, and results prove its feasibility.

Keywords: Vibro-impact, Optimal design, Activation, Nonlinear system, Targeted energy transfer, Nonlinear energy sink, Impact damper

*Corresponding author

Email addresses: tli@insa-toulouse.fr (T. Li), qiu@insa-toulouse.fr (D. Qiu), sebastien.seguy@insa-toulouse.fr (S. Seguy), alain.berlioz@univ-tlse3.fr (A. Berlioz)

1. Introduction

In engineering, clearance is common for structures such as linkage, gear train and joint. Impacts come into being when two objects contact, and can result in energy transfer and dissipation. This phenomenon is applied to vibration control since seventy years ago [1] and an auxiliary device is termed as impact damper. Later, there are extensive studies around impact damper and its dynamics as a typical vibro-impact system [2, 3]. The focus here is put on some recent studies since they are tightly related to the work of this paper.

Recently, impact damper is re-examined under the context of Targeted Energy Transfer (TET) [4, 5] and called Vibro-Impact (VI) Nonlinear Energy Sink (NES) [6, 7, 8]. The main advance comes from the analytical study of underlying Hamiltonian system [9] and the application of multiple scales method [10]. Consequently, special orbits that lead to TET are found from the former, and a Slow Invariant Manifold (SIM) that controls the variation of resonance captures are obtained from the latter. Some following analytical and numerical studies reveal further information about the complicated dynamics of this VI system, especially Strongly Modulated Response (SMR) [11, 12] and bifurcation analysis from the perspective of impact time difference [13].

In addition to the explanation of its dynamics, there are also many researches about its characteristic as a damper. In general, two aspects of study results are obtained [8, 9], namely activation characteristic and parameter optimization. In terms of activation, VI NES is observed to respond fast at an initial stage when a main system is perturbed, and it is effective in a broad frequency range from the results of frequency spectrum analysis. With respect to parameter design, many suggestions are proposed, for example a medium clearance is better. Around these two aspects, it is found that the impact number per cycle of a main system matters for energy transfer and dissipation [14]. Then, the efficiency of different response regimes with different impact number per cycle is compared in [15], and it is found that the limit between response with permanent two impacts per cycle and that with intermittent two impacts per cycle (SMR) is optimal. Its essence behind is transient resonance captures with two impacts per cycle. This conclusion also holds for a linear system coupled with two VI NES in parallel [16]. In [15], there is another interesting phenomenon, just a range of clearance will be effective for a fixed outside excitation. Equivalently, a fixed clearance will only be effective in a displacement amplitude range of a main system [16].

This feature is very interesting in terms of vibration control and is very special as a NES. In [17], this kind of characteristic is also tried to be designed for a

nonlinear vibration absorber but in a general way. Its basic philosophy of design can be reflected by the response regime with two impacts per cycle of systems coupled with VI NES.

Whether this effective activation of VI NES only depends on the displacement amplitude and has nothing to do with frequency? If the answer is positive, it could be applied as a design criterion for VI NES to control the vibration of nonlinear systems at some displacement levels. Its benefit is evident since it maybe impossible to get reliable results from analytical studies of nonlinear systems coupled with VI NES, and the above-mentioned idea may provide a feasible solution.

The difficulty of the application of NES to control vibration is already observed. For example, VI NES is attached to a cutting tool to quench its chatter in [18]. Experimental results demonstrate that an appropriately designed VI NES can effectively reduce the vibration of a cutting tool. However, its analytical development is based on a simplified equation and still has a distance to predict real responses, which is the same case for a turning system coupled with a cubic NES [19]. The problem is the same for a helicopter [20, 21]. Considering the difficulty of analytical study for any nonlinear systems coupled with VI NES, the possibility to apply its activation characteristic and to simplify its design for nonlinear systems will be explored.

The paper is organized as follows. In Section 2, a theoretical analysis for the activation characteristic of VI NES is presented. In Section 3 and 4, this activation characteristic is validated by numerical and experimental results from different linear and nonlinear main systems, respectively. In Section 5, a design procedure of VI NES is proposed and applied to control chatter in turning. Finally, conclusion is addressed.

2. Analytical treatment

In essence, the analytical development here is similar to that of former studies [10, 11, 14], but some important information of SIM is neglected and will be further analyzed.

2.1. Analytical formulation

[**Fig.** 1 about here.]

A LO under periodic excitation and coupled with a VI NES is showed in Fig. 1. Its motion between impacts is described by the following equation:

$$
\begin{aligned}
&\ddot{x}+\varepsilon\lambda_1\dot{x}+x=\varepsilon G\sin\Omega\tau+\varepsilon^2\lambda_1 G\Omega\cos\Omega\tau\\
&\varepsilon\ddot{y}=0\\
&\forall\,|x-y|<b
\end{aligned}
\tag{1}
$$

Parameters are expressed as follows:

$$
\begin{aligned}
&\varepsilon=\frac{m_2}{m_1},\quad {\omega_0}^2=\frac{k_1}{m_1},\quad f_0=\frac{\omega_0}{2\pi},\quad \tau=\omega_0 t,\\
&\lambda_1=\frac{c_1}{m_2\omega_0},\quad \Omega=\frac{\omega}{\omega_0},\quad G=\frac{F}{\varepsilon}
\end{aligned}
$$

where x, m_1, c_1 and k_1 are the displacement, mass, damping and stiffness of LO, respectively. y and m_2 represent displacement and mass of VI NES, respectively. Dots denote differentiation with respect to dimensionless time τ. b represents the clearance. $x_e(t)$ is the displacement imposed on the base by a shaker. $\varepsilon G\sin\Omega\tau$ and $\varepsilon^2\lambda_1 G\Omega\cos\Omega\tau$ represent the force contribution of displacement and that of velocity by outside excitation, respectively. The latter term is conserved here to demonstrate its physical meaning and is neglected during the following analysis because of its small magnitude.

When $|x-y|=b$, impacts occur. The relation between after and before impact is obtained under the hypothesis of simplified shock theory and the condition of momentum conservation:

$$
\begin{aligned}
&x^+=x^-,\quad y^+=y^-\\
&\dot{x}^++\varepsilon\dot{y}^+=\dot{x}^-+\varepsilon\dot{y}^-,\quad \dot{x}^+-\dot{y}^+=-r\left(\dot{x}^--\dot{y}^-\right),\\
&\text{for } |x-y|=b
\end{aligned}
\tag{2}
$$

where r is the restitution coefficient, and the superscripts $+$ and $-$ indicate the time immediately after and before impact. New variables representing the displacement of the center of mass and the internal displacement of VI NES are introduced:

$$
v=x+\varepsilon y,\quad w=x-y \tag{3}
$$

Substituting Eq. (3) into Eqs. (1) and (2), the equation between impacts in barycentric coordinate is given as:

$$
\begin{aligned}
&\ddot{v}+\varepsilon\lambda_1\frac{\dot{v}+\varepsilon\dot{w}}{1+\varepsilon}+\frac{v+\varepsilon w}{1+\varepsilon}=\varepsilon G\sin\Omega\tau+\varepsilon^2\lambda_1 G\Omega\cos\Omega\tau\\
&\ddot{w}+\varepsilon\lambda_1\frac{\dot{v}+\varepsilon\dot{w}}{1+\varepsilon}+\frac{v+\varepsilon w}{1+\varepsilon}=\varepsilon G\sin\Omega\tau+\varepsilon^2\lambda_1 G\Omega\cos\Omega\tau\\
&\forall|w|<b
\end{aligned}
\tag{4}
$$

and the impact condition (2) is rewritten as:

$$
\begin{aligned}
&v^+=v^-,\quad w^+=w^-,\\
&\dot{v}^+=\dot{v}^-,\quad \dot{w}^+=-r\dot{w}^-,\quad \text{for } |w|=b
\end{aligned}
\tag{5}
$$

Multiple scales are introduced in the following form:

$$
\begin{aligned}
&v(\tau;\varepsilon)=v_0(\tau_0,\tau_1,\ldots)+\varepsilon v_1(\tau_0,\tau_1,\ldots)+\ldots\\
&w(\tau;\varepsilon)=w_0(\tau_0,\tau_1,\ldots)+\varepsilon w_1(\tau_0,\tau_1,\ldots)+\ldots\\
&\tau_k=\varepsilon^k\tau,\quad k=0,1,\ldots
\end{aligned}
\tag{6}
$$

A detuning parameter (σ) representing the nearness of the forcing frequency Ω to the simplified natural frequency of LO is introduced:

$$
\Omega=1+\varepsilon\sigma \tag{7}
$$

Substituting Eqs. (6) and (7) into Eqs. (4) and (5), equating coefficients of like power of ε and only conserving the first two orders:

Order ε^0:

$$
\begin{aligned}
&D_0^2v_0+v_0=0\\
&D_0^2w_0+v_0=0,\quad \forall|w_0|<b
\end{aligned}
\tag{8}
$$

$$
\begin{aligned}
&v_0^+=v_0^-,\quad w_0^+=w_0^-,\\
&D_0v_0^+=D_0v_0^-,\quad D_0w_0^+=-rD_0w_0^-,\quad \text{for } |w_0|=b
\end{aligned}
\tag{9}
$$

Order ε^1:

$$
\begin{aligned}
D_0^2v_1+v_1=&-2D_0D_1v_0-\lambda_1D_0v_0-w_0+v_0\\
&+G\sin(\tau_0+\sigma\tau_1)
\end{aligned}
\tag{10}
$$

where D_0 represents partial derivative to time τ_0. For order ε^1, only the term related to LO is conserved and will be used later. Combining the first order and the second one, both SIM and fixed points could be obtained. From the analysis

of order ε^0, v_0 represents an ideal undamped harmonic oscillator expressed as follows:

$$v_0 = C(\tau_1)\sin(\tau_0 + \theta(\tau_1)) \tag{11}$$

where $C(\tau_1)$ and $\theta(\tau_1)$ are its amplitude and phase, respectively. From the standpoint of w_0, Eq. 8 and Eq. 9 represent a harmonically forced impact oscillator with symmetric barrier. For the response regime (1 : 1 resonance) with two impacts per cycle, its solution can be searched in the following form:

$$w_0 = C(\tau_1)\sin(\tau_0 + \theta(\tau_1)) + \frac{2}{\pi}B(\tau_1)\Pi(\tau_0 + \eta(\tau_1)) \tag{12}$$

where $B(\tau_1)$ and $\eta(\tau_1)$ are displacement amplitude and phase of VI NES, respectively. $\Pi(z)$ is a non-smooth sawtooth function [22]. This folded function and its derivative are depicted in Fig. 2 and expressed as follows:

[**Fig.** 2 about here.]

$$\Pi(z) = \arcsin(\sin z), \quad M(z) = \frac{d\Pi}{dz} = sgn(\cos z) \tag{13}$$

According to Eqs. (12) and (13), impact occurs at $T_0 = \pi/2 - \eta + j\pi$ with $j = 0, 1, 2, \ldots$. The impact condition $|w_0| = b$ is rewritten with Eq. (12) as:

$$C\cos(\eta - \theta) = b - B \tag{14}$$

Rewriting now the inelastic impact condition Eq. (9) yields:

$$C(1+r)\sin(\eta - \theta) = \frac{2}{\pi}B(1-r) \tag{15}$$

Combining Eqs. (14) and (15), a relation between B and C is obtained as follows:

$$C^2 = \left(1 + \frac{4(1-r)^2}{\pi^2(1+r)^2}\right)B^2 - 2bB + b^2 \tag{16}$$

An example of SIM described by Eq. (16) with $b = 1$ and $r = 0.6$ is presented in Fig. 3. The stability of SIM is analyzed by an asymptotic approach used in [11] that is originally applied in [23, 24]. By this stable analysis method, the stable branch is defined by the condition that the modulus of all the eigenvalues of

a certain matrix relating two consecutive impacts is less than unity. This stability analysis can also be accomplished by direct numerical integration of Eqs. (8) and (9).

[**Fig.** 3 about here.]

In order to obtain fixed points or study the non-stationary evolution of the motion of the system on the SIM, i.e., the analysis of transient resonance captures under transient excitation and transient resonance captures of SMR, Eq. (10) at the next order of approximation is analyzed. To identify terms that produce secular terms, the function of w_0 is expanded in Fourier series:

$$\begin{aligned} w_0 =& C(\tau_1)\sin(\tau_0+\theta(\tau_1))+E(\tau_1)\sin(\tau_0+\zeta(T_1)) \\ &+\mathrm{RFC} \end{aligned} \tag{17}$$

where RFC represents the rest components in addition to the simplified natural frequency of LO. The component $C(\tau_1)$ is decided by the motion of LO and $E(\tau_1)$ is totally related to the motion of VI NES. The value of $E(\tau_1)$ is related to the periodic impact force. The Eq. (17) is a more general and relaxed analytical description with respect to the motion of VI NES compared to former studies [10, 11] that consider only 1:1 resonance with two symmetric impacts per cycle.

Substituting Eqs. (11), (12) and (17) into Eq. (10) and eliminating terms that produce secular terms give:

$$\begin{aligned} D_1 C &= -\frac{1}{2}\lambda_1 C - \frac{1}{2}E\sin(\Theta)+\frac{1}{2}G\sin(\eta) \\ D_1\eta &= \frac{1}{2}G\cos(\eta)/C - \frac{1}{2}E\cos(\Theta)/C+\sigma \end{aligned} \tag{18}$$

where

$$\begin{aligned} \Theta &= \zeta-\theta \\ \eta &= \sigma\tau_1-\theta \end{aligned} \tag{19}$$

Θ represents the phase difference related to LO and VI NES. η represents the phase difference related to LO and outside excitation.

The fixed points can be obtained by equating the left side of Eq. (18) to zero and then combining it with Eq. (16). In this way, the fixed points (number and position) can be obtained. Compared to the classic non-asymptotic method, the functionality of this asymptotic method is twofold. Firstly, the position of points can be used to judge the type of response regime. Secondly, values can be precisely calculated for 1:1 resonance, which is related to optimal response regime

[15]. Meanwhile, the corresponding equivalent force E between LO and VI NES can be used to analyze their underlying dynamic performance.

2.2. Analysis of SIM

For a fixed point in SIM as showed in Fig. 3, C and B represent the displacement amplitude related to LO and VI NES, respectively. After a dimensionless process, these two parameters remain the same. However, the frequency of LO is normalized and the velocity of VI NES is also scaled. It means that one point of SIM actually represents different response regimes which have the same ratio between C and B but possess different frequencies. Different points of SIM represent different responses with different ratios of displacement amplitude and they together represent all possible response regimes. Here, one important point that different systems coupled with a same VI NES can have the same SIM is neglected during all former studies, because these former studies are carried out for different systems case by case.

In [15], it is found that a VI NES with a specific clearance will only be effective in a range of displacement amplitude of LO. Actually, this is related to the blue stable branch of SIM in Fig. 3. Theoretically, VI NES with a fixed clearance should be activated at a fixed displacement amplitude interval for different LO with different natural frequencies. Then, whether it still holds for nonlinear systems with varying frequency when its energy changes. If a considered nonlinear system at different energy levels can be equivalent to different linear systems with different frequencies, the above activation characteristic can still be used. The essence behind is to find the activation condition of VI NES. In this way, the difficulty of analytical treatment of system coupled with VI NES during the design process can be avoided.

To design VI NES for vibration control of a nonlinear system, actually it is difficult to get the full information of this nonlinear system, let alone to treat this coupled system analytically. However, its range of work displacement amplitude is normally known in advance or can be obtained from a design objective. From the above analysis, it is exactly what needed for the optimal or relatively optimal design of VI NES.

2.3. A design procedure for VI NES coupled to nonlinear systems

For the design of a VI NES for the vibration control of a nonlinear system, the idea is simple and just to find a similar linear system to this nonlinear system, then to optimally design VI NES for this linear system. However, there are some requirements to assure VI NES still works for target nonlinear system. Firstly and

at least, the amplitude of this linear system should be the same as that of nonlinear system. Secondly and unnecessarily, the frequency of this linear system should be designed the same as that of nonlinear system. If just a linear system is used to approximate this nonlinear system working in a range of displacement amplitude, usually only the amplitude range can be approximated by this linear system and the condition with same frequency cannot be met. This requires a prerequisite that VI NES will be activated at a range of amplitude and its activation is independent of frequency. This point will be investigated in the following section.

As a summary, the activation of VI NES as a damper is special from two perspectives. Firstly, a VI NES with a fixed clearance will only be effective in a range of displacement amplitude. It means that different clearances will be activated at different amplitudes of displacement as observed from experimental transient excitation results [16]. This characteristic is very important in the domain of vibration control. The second characteristic is about its effectiveness in a broad frequency range. Former observations are based on the frequency spectrum analysis of a transient or periodic response, and this way is indirect. This time, its theoretical base is well demonstrated from the analysis of SIM.

3. Numerical observations

To guarantee the above-mentioned design mechanism of VI NES for nonlinear systems, several aspects about activation characteristics of VI NES will be checked in this section. Firstly, critical points (i.e., p0, p1 and p2) of SIM should have the same values for different linear or nonlinear systems with different frequencies under some same conditions. For this purpose, three linear systems with different natural frequencies and one Duffing system with cubic nonlinearity are numerically studied. Moreover, whether an optimal clearance of VI NES for one system is still optimal for other systems is investigated. Secondly, the proportional activation of VI NES with different clearances is experimentally examined.

3.1. LO and Duffing systems

Eq. (1) is modified to Eq. (20) in order to include a cubic term described by α, and a proportional factor β is introduced to regulate linear stiffness. The variation of β will be reflected in parameter λ_1. For moments of impact, Eq. (2) still applies. The meaning of other parameters is the same as those in the last section. Eqs. (20) and (2) will be combined for numerical simulation, and the following parameters are fixed except specially pointed out: $\varepsilon = 0.84, r = 0.6$.

$$\begin{aligned} &\ddot{x}+\varepsilon\lambda_1\dot{x}+x+\alpha x^3=\varepsilon G\sin\Omega\tau+\varepsilon^2\lambda_1 G\Omega\cos\Omega\tau \\ &\varepsilon\ddot{y}=0 \\ &\forall|x-y|<b \end{aligned} \tag{20}$$

where

$$\omega_0{}^2=\frac{\beta k_1}{m_1}$$

3.2. Free vibration of LO with different natural frequencies

The following parameters and initial conditions are used: $G=0,\alpha=0,b=0.05,x_0=0.1,\dot{x_0}=0,y_0=b,\dot{y_0}=0$. The following three values β are consecutively chosen: 1, 0.75 and 0.5. The objective is to create three different linear systems.

The results are showed in Fig. 4. For $\beta=1$, the displacement of LO and relative displacement are displayed in Figs. 4 (a) and (b), respectively. Then, two points and their values are marked out in Figs. 4 (c-d). They correspond to special points p0 and p2 in Fig. 3. Because the transition from regime with two asymmetric impacts per cycle to the symmetric case is difficult to distinguish, only p0 and p2 are used in the following results. In Fig. 4(e), corresponding value x of p0 and p2 for these three different β is compared. These two broken lines are the line fitting of numerical results. It is observed that the value x is almost the same for these three values of β.

[**Fig.** 4 about here.]

When parameters and initial conditions are fixed as: $G=0,\beta=1,\alpha=0,x_0=0.02,\dot{x_0}=0,y_0=b,\dot{y_0}=0$, different values of b are chosen to compare its efficiency for a same main system and $b=0.05$ is found to be optimal. Then this optimal value of b is applied to other systems with different β. The results are demonstrated in Fig. 5. The time history of displacement for $\beta=1$ is displayed in Fig. 5(a) and x related to $p2$ is marked out. The comparison between three different β is showed in Fig. 5(b) . All three values are around 0.0052, which results in almost the same decay inclination for these three systems.

[**Fig.** 5 about here.]

3.3. Free vibration of different Duffing systems

For systems with cubic nonlinearity, the following parameters and initial conditions are used: $G = 0, \alpha = 250000, \beta = 1, x_0 = 0.02, \dot{x_0} = 0, y_0 = b, \dot{y_0} = 0$. Different values of b are chosen to compare their efficiency. x related to p2 are compared and showed in Fig. 6. It is observed that x for p2 is proportional to b, and this characteristic will also be demonstrated in the following experimental results.

[**Fig.** 6 about here.]

As a summary, it is numerically observed the proportional activation of VI NES to different clearances and the independence of its activation to the frequency of main systems.

4. Experimental observations

The objective of this section is to verify the activation of VI NES from different experimental results under different excitations.

4.1. Periodic excitation

For periodic excitation, experiments for a LO coupled with a VI NES are the same as these in [15], in which specific information about experimental configuration and parameters can be found. Here, just the time history of displacement is demonstrated for a single frequency excitation at the first place, and for a range of frequency at the second place.

4.1.1. Single frequency excitation

The whole time histories of displacement of LO for three different b is showed in Fig. 7 (a-c) , respectively. Judging from the time range $20-70$ s, SMR occurs at this stable area, and the point of minimal amplitude related to p2 is marked out at the same time moment for all three of them. Its value denoted by Y is marked out. The relation between different b and its corresponding minimal amplitude is represented by blue circles in Fig. 7(d) and then is linearly interpolated. The consistency between the red broken line and circles proves the proportional activation characteristic to some extent considering that the number of points is limited. However, this activation feature could be further observed from other viewpoints.

[**Fig.** 7 about here.]

4.1.2. Excitation with a band of frequency

To observe the proportional activation characteristic of VI NES, the amplitude of LO related to the limit point p2 in SIM, i.e., the corresponding response regime limit between SMR and two impacts per cycle, is recorded for different values of b during the sweep process.

[**Fig.** 8 about here.]

The displacement amplitudes of LO are marked out for different b and showed in Fig. 8(a) and (b). The shift of resonance peak between different experimental results comes from the difference of the starting record time. The starting or ending points of the regime with two impacts per cycle are marked out for different b and their specific judgment requires the data of acceleration. This judgment process will be demonstrated for the analysis of the following transient experimental results. It should be pointed out here that these marked points are enough to coarsely describe the difference caused by b, though it is difficult to accurately locate these points. Moreover, these two points entering into and leaving from the regime with two impacts per cycle is visible and distinguishable during the experimental process. As has been done before, these points are fitted by a red broken line as showed in Fig. 8(c). These points almost locate in a line and prove again the proportional activation characteristic.

4.2. Transient excitation

The objective of transient experiments with different linear and nonlinear systems is to study whether the activation of VI NES is related to frequency.

4.2.1. Experimental configuration

[**Fig.** 9 about here.]

In addition to the above experimental results under periodic excitation, three linear systems with different stiffness and one Duffing system are experimentally studied under transient excitation. The objective here is to observe the dependence of the activation behavior of VI NES on frequency. More specifically, it is to test that a VI NES with a same clearance will be excited at a same displacement range of a main system with different frequencies.

[Table 1 about here.]

The same mass and damping of oscillator, same VI NES as showed in Fig. 9 will be used during the whole experimental process. Only the number of springs is changed from 4 to 3 or 2, or even the direction of springs is changed to create a Duffing system. The oscillator is installed to a cast iron bench, and its displacement and acceleration are measured by an acceleration sensor and a displacement sensor, respectively. The LO is detailed in Fig. 9(a) and its stiffness can be regulated by modifying the number of springs in its two sides. A detailed view of the fixation of springs is displayed in Fig. 9(b), in which two springs are used. If only one spring is used, this spring will be attached to middle holes. During the experimental process, 4, 3 and 2 springs are consecutively applied. Their stiffness can be calculated according to the value of 4 springs as showed in Table 1. The device to regulate displacement is showed in Fig. 9(c) and the initial displacement of LO is set to around 20 mm for all tests. An enlarged view of VI NES is demonstrated in Fig. 9(d). Its initial location is random for all tests. The specific location is not so important, since only the stable process will be considered. In addition, the initial velocities of LO and VI NES are zero. A Duffing system is showed in Fig. 9(e). It should be pointed out that only the stiffness is different for the above four systems.

[**Fig.** 10 about here.]

4.2.2. Experimental results

The response for LO with 4 springs and $b = 5$ mm is demonstrated in Fig. 10 to illustrate the process to identify typical values related to two limit points p0 and p2. The first limit point is that between the regime with three impacts per cycle and that with two impacts per cycle, and the second is the one between the regime with two impacts per cycle and that with less than two impacts per cycle. The displacement is showed in Fig. 10(a), the first limit is between two points: the local maximum point A2 and minimum point A3. Similarly, the second limit point is between two other points: the local maximum point B2 and minimum point B3. The identification of these four points can be obtained from special points at the time history of acceleration in Fig. 10(b) and this identification is also used for the former periodic experimental results. Two periods are enlarged and displayed in Fig. 10(c) and (d). Point A1 is the last impact of periods with three impacts per cycle. Point B1 is the last impact of the regime with two impacts per cycle. According to values of A1 and B1, special points A2, A3, B2 and B3 can be identified, and then corresponding displacement amplitudes of this main oscillator can be obtained, as showed in Fig. 10(a).

[**Fig.** 11 about here.]

For different main systems with same displacement amplitude, its energy is bigger for a larger stiffness. For free vibration, there exist more oscillations during the decay process for the case with larger stiffness. Therefore, it will be clearer to see the transition process of different transient response regimes with a larger stiffness for the same VI NES, since the transition process of transient response is finer.

[**Fig.** 12 about here.]

Then, amplitudes related to these two limit points p0 and p2 for four different main systems are compared and showed in Fig. 12. As showed in Fig. 12(a), the first three values in the horizontal axis represent LO with 4, 3 and 2 springs, respectively. The last value represents a Duffing system with 4 springs. The meaning of the horizontal axis is the same for other three subfigures. Two clearances $b = 5$ mm and 10 mm are chosen and results are showed in Fig. 12(a-b) and Fig. 12(c-d), respectively. Broken lines are curve fittings of experimental data to show its variation trend. In Fig. 12(a), the results are obtained from positive amplitude of displacement, A2 and A3 illustrate the first and second limit points, respectively. The values of x are almost the same compared to its absolute value, which provides a direct proof that the activation characteristic of VI NES is independent of frequency. A small increase of value with the decrease of the number of springs is reasonable because the representation of transient responses by measured data becomes coarse with the decrease of stiffness. As for the comparison between LO with 2 springs and Duffing system with 4 springs, the difference is not significant because that their stiffness are close and other unclear factors like friction may play a critical role in deciding this value.

The same conclusion can be obtained from the analysis of points A3 and B3 in the negative side of displacement as showed in Fig. 12(b). Moreover, results showed in Fig. 12(c-d) for $b = 10$ mm also support the above analysis.

In summary, activation characteristic of VI NES is examined from experimental viewpoints, and there are some credible results for its proportional activation. In addition, the dependence of its activation on frequency is explored by a transient experiment. Although there are some results credible to some extent, they are not so ideal and it results from the fact that the frequency difference between these four systems is not large enough, meanwhile limit points p0 and p2 can not be truly accurately obtained for these four systems with low frequency.

5. Design of VI NES for chatter control

In this section, a design procedure of VI NES based on its activation characteristic will be applied to control the chatter of a cutting tool during a turning process. A simplified model and corresponding experimental parameters in [18] will be used. The application of VI NES has been experimentally observed to be efficient in quenching an unstable cutting in this paper. It is demonstrated that the bifurcation diagram is complex [25] and corresponding response regimes are also complex. Two typical cases will be chosen to demonstrate this optimization procedure. One case corresponds to an unstable cutting possessing a steady state response as well as a stable cutting with zero amplitude. The other case corresponds to an unstable cutting characterized by beating response.

5.1. Model of a cutting tool coupled with VI NES

[**Fig.** 13 about here.]

A simplified model of a cutting tool coupled with a VI NES is represented in Fig. 13. The cutting tool is supposed to only vibrate in the feed direction and the workpiece is considered rigid. The corresponding equation of motion between impacts is written as follows:

$$\begin{aligned} &m_1\ddot{x}+c_1\dot{x}+k_1x+k_2x^3=F_x \\ &F_x=p(\rho_1\Delta h^1+\rho_2\Delta h^2+\rho_3\Delta h^3) \\ &\varepsilon\ddot{y}=0 \\ &\forall\,|x-y|<b \end{aligned} \tag{21}$$

[Table 2 about here.]

Related parameters are expressed as follows:

$$\omega_0{}^2=\frac{k_1}{m_1},\quad f_1=\frac{\omega_0}{2\pi},\quad \mu_1=\frac{c_1}{2m_2\omega_0} \tag{22}$$

where x, m_1, c_1, k_1 and k_3 are the displacement, mass, damping, coefficient of linear stiffness and coefficient of cubic stiffness of the cutting tool, respectively. y and m_2 are displacement and mass of VI NES. Dots denote the differentiation with respect to time t. Δh is decided by the current displacement and the displacement trajectory left by the last pass. b represents the clearance. When $|x-y|=b$, impacts occur. The relation between after and before impact is obtained under the

hypothesis of simplified shock theory and the condition of momentum conservation:

$$\begin{aligned} &x^+ = x^-, \quad y^+ = y^- \\ &m_1\dot{x}^+ + m_2\dot{y}^+ = m_1\dot{x}^- + m_2\dot{y}^-, \\ &\dot{x}^+ - \dot{y}^+ = -r\left(\dot{x}^- - \dot{y}^-\right), \\ &\text{for } |x-y| = b \end{aligned} \tag{23}$$

[**Fig.** 14 about here.]

5.2. Design of VI NES for different cases

Physical and cutting parameters are showed in Table 2. Only the cutting width h_0 and clearance b will be varied. At first, the system is not coupled with VI NES and the cutting width is varied to see the bifurcation process. When $h_0 = 0.11$ mm, a case with two fixed points is observed denoted as case 1 and another fixed point with beating response is located with $h_0 = 0.16$ mm and is denoted as case 2. The response regimes for these two cases without and with VI NES will be demonstrated.

5.2.1. Case 1

For $h_0 = 0.11$ mm, the following initial conditions are fixed and used: $\dot{x_0} = 0, y_0 = b, \dot{y_0} = 0$. Only initial displacement x_0 is changed. When x_0 is chosen to a large enough value such as 0.20 mm and 0.01 mm, x will be attracted to a same steady state, which corresponds to an unstable cutting as showed in Fig. 14(a) and (b), respectively. If the initial condition is small enough, the response will decay to zero as displayed in Fig. 14(c).

To design b for VI NES, the analytical results in Section 2 will be used. At first, a LO close to this cutting tool, i.e., with the same displacement amplitude, is created. In addition, the corresponding LO will possess other same characteristics as the cutting tool as many as possible. The frequency of outside excitation for this created linear oscillator is fixed to the experimentally obtained frequency f_0 and its amplitude will be chosen in order that the displacement amplitude of LO will be the same as that of the cutting tool. Then b is designed to make the target displacement amplitude of LO locate in p2 of the corresponding SIM under periodic excitation and in p1 for transient excitation. For the cutting tool, its final steady state, i.e., a steady non-zero or zero amplitude, is applied to decide which points will be chosen.

[**Fig.** 15 about here.]

For the first two initial conditions, response of the cutting tool is periodic and its amplitude is $5.41 * 10^{-3}$ mm and b is chosen to p2. For the third initial condition, response is transient and its displacement amplitude at the starting point $2.199 * 10^{-3}$ mm is chosen to make it locate at p1. The effect with VI NES is demonstrated in Fig. 15. For the first two initial conditions, the unstable state is improved to a stable state and its vibration is completely controlled as showed in Fig. 15(a-b). Meanwhile, its transient process of energy dissipation is accelerated. This is the same case for the third initial condition as showed in Fig. 15(c).

5.2.2. Case 2

[**Fig.** 16 about here.]

Compared to case 1, a beating response occurs for $h_0 = 0.16$ mm as represented by the blue curve in Fig. 16(a). Its amplitude of displacement is not steady. If the relative maximal value of point T1 is chosen as the target to create LO, the estimated amplitude will be high, and the response should be designed according to p1 with a relative high clearance for VI NES. In return, it will be a little small for the relative minimal value of point T2, the response should be designed according to p2.

When the relative minimal value $Y = 3.208 * 10^{-3}$ mm of T2 is chosen, the p1 is used as the targeted point. The result is showed in Fig. 16(a) and the displacement of the cutting tool in red curve is almost zero in this case. When the relative maximal value $Y = 1.14 * 10^{-2}$ mm of point T1 is chosen with p2 as the target. The result in red curve is showed in Fig. 16(c) and the displacement of cutting tool is greater with this b. The displacement of VI NES y for these two designed values are showed in Figs. 16(b) and (d), respectively. For the first value of b, VI NES is much more activated at the beginning. Once vibration is decreased to a little value, VI NES is no longer activated. For the second value in Fig. 16 (d), VI NES is also activated, but its vibration is not reduced as the first value and VI NES is just occasionally activated.

In summary, the design procedure proposed for VI NES is feasible and effective for unstable cuttings during turning process. It demonstrates the feasibility of relatively optimal design of VI NES for vibration control of nonlinear systems.

6. Conclusion

IIn this paper, SIM obtained from analytical development of LO coupled with VI NES is further analyzed. Activation characteristic of VI NES as a damper is

analyzed from SIM and applied for design of VI NES. Then, activation characteristic of VI NES is numerically and experimentally validated. Finally, a proposed design procedure of VI NES is applied to control the chatter during a turning process.

Although SIM has been greatly analyzed during the analytical treatment of system coupled with VI NES, its relation to frequency is not clearly explained before. It is found that VI NES with a clearance will be activated in a fixed range of displacement amplitude of a main system. Moreover it will not be affected by the frequency of this main system. Two highlights are obtained. Firstly, the effectiveness of VI NES in a broad range of frequency of a main system can be viewed from another direct viewpoint, namely analytical viewpoint, and this idea is different from traditional perspectives. Secondly, each NES could possess its own characteristic and need special attention.

The design procedure of VI NES for the chatter control of a turning process is just applied to demonstrate the way to design VI NES for vibration control of nonlinear systems. Therefore, this section appears short and needs further study later.

In general, about the activation characteristic of VI NES obtained from analytical analysis, the experimental results are general credible and prove the analytical results. But they are not so ideal, for example, when Duffing system is created, the stiffness of cubic term is so week that a significant change of frequency to assure comparison cannot be obviously observed.

Acknowledgments

The authors acknowledge the French Ministry of Science and the Chinese Scholarship Council [grant number: 201304490063] for their financial support.

References

[1] P. Lieber, D. Jensen, An acceleration damper: development, design and some applications, Trans. ASME 67 (10) (1945) 523–530.

[2] R. A. Ibrahim, Vibro-impact dynamics: modeling, mapping and applications, Vol. 43, Springer Science & Business Media, Berlin, 2009.

[3] V. I. Babitsky, Theory of vibro-impact systems and applications, Springer Science & Business Media, Berlin, 2013.

[4] Y. Lee, A. F. Vakakis, L. Bergman, D. McFarland, G. Kerschen, F. Nucera, S. Tsakirtzis, P. Panagopoulos, Passive non-linear targeted energy transfer and its applications to vibration absorption: a review, Proceedings of the Institution of Mechanical Engineers, Part K: Journal of Multi-body Dynamics 222 (2) (2008) 77–134.

[5] A. F. Vakakis, O. Gendelman, L. Bergman, D. McFarland, G. Kerschen, Y. Lee, Nonlinear targeted energy transfer in mechanical and structural systems, Vol. 156, Springer Science & Business Media, Berlin, 2008.

[6] F. Nucera, A. Vakakis, D. McFarland, L. Bergman, G. Kerschen, Targeted energy transfers in vibro-impact oscillators for seismic mitigation, Nonlinear Dynamics 50 (3) (2007) 651–677.

[7] F. Nucera, F. Lo Iacono, D. McFarland, L. Bergman, A. Vakakis, Application of broadband nonlinear targeted energy transfers for seismic mitigation of a shear frame: Experimental results, Journal of Sound and Vibration 313 (1) (2008) 57–76.

[8] I. Karayannis, A. Vakakis, F. Georgiades, Vibro-impact attachments as shock absorbers, Proceedings of the Institution of Mechanical Engineers, Part C: Journal of Mechanical Engineering Science 222 (10) (2008) 1899–1908.

[9] Y. Lee, F. Nucera, A. Vakakis, D. McFarland, L. Bergman, Periodic orbits, damped transitions and targeted energy transfers in oscillators with vibro-impact attachments, Physica D: Nonlinear Phenomena 238 (18) (2009) 1868–1896.

[10] O. Gendelman, Analytic treatment of a system with a vibro-impact nonlinear energy sink, Journal of Sound and Vibration 331 (2012) 4599–4608.

[11] E. Gourc, G. Michon, S. Seguy, A. Berlioz, Targeted energy transfer under harmonic forcing with a vibro-impact nonlinear energy sink: Analytical and experimental developments, Journal of Vibration and Acoustics 137 (3) (2015) 031–008.

[12] O. Gendelman, A. Alloni, Dynamics of forced system with vibro-impact energy sink, Journal of Sound and Vibration 358 (2015) 301–314.

[13] T. Li, S. Seguy, A. Berlioz, On the dynamics around targeted energy transfer for vibro-impact nonlinear energy sink, Nonlinear Dynamics 87 (3) (2017) 1453–1466.

[14] T. Li, S. Seguy, A. Berlioz, Dynamics of cubic and vibro-impact nonlinear energy sink: Analytical, numerical, and experimental analysis, Journal of Vibration and Acoustics 138 (3) (2016) 031–010.

[15] T. Li, S. Seguy, A. Berlioz, Optimization mechanism of targeted energy transfer with vibro-impact energy sink under periodic and transient excitation, Nonlinear Dynamics 87 (4) (2017) 2415–2433.

[16] T. Li, E. Gourc, S. Seguy, A. Berlioz, Dynamics of two vibro-impact nonlinear energy sinks in parallel under periodic and transient excitations, International Journal of Non-Linear Mechanics 90 (2017) 100 – 110.

[17] R. Viguié, G. Kerschen, Nonlinear vibration absorber coupled to a nonlinear primary system: a tuning methodology, Journal of sound and Vibration 326 (3) (2009) 780–793.

[18] E. Gourc, S. Seguy, G. Michon, A. Berlioz, B. Mann, Quenching chatter instability in turning process with a vibro-impact nonlinear energy sink, Journal of Sound and Vibration 355 (2015) 392–406.

[19] E. Gourc, S. Seguy, G. Michon, A. Berlioz, Chatter control in turning process with a nonlinear energy sink, in: Advanced Materials Research, Vol. 698, Trans Tech Publ, 2013, pp. 89–98.

[20] E. Gourc, L. Sanches, G. Michon, V. Steffen, Post-critical analysis of ground resonance phenomenon: effect of stator asymmetry, Nonlinear Dynamics 83 (1) (2016) 201–215.

[21] B. Bergeot, S. Bellizzi, B. Cochelin, Analysis of steady-state response regimes of a helicopter ground resonance model including a non-linear energy sink attachment, International Journal of Non-Linear Mechanics 78 (2016) 72–89.

[22] V. Pilipchuk, Closed-form solutions for oscillators with inelastic impacts, Journal of Sound and Vibration 359 (2015) 154–167.

[23] S. Masri, T. Caughey, On the stability of the impact damper, Journal of Applied Mechanics 33 (3) (1966) 586–592.

[24] C. Bapat, N. Popplewell, K. McLachlan, Stable periodic motions of an impact-pair, Journal of Sound and Vibration 87 (1) (1983) 19–40.

[25] A. H. Nayfeh, N. A. Nayfeh, Analysis of the cutting tool on a lathe, Nonlinear Dynamics 63 (3) (2011) 395–416.

List of Tables

List of Figures

Table 1. Experimental parameters [15]

Physical Parameters			
m_1	4.7 kg	c_1	3.02 Ns/m
k_1	$11.47 * 10^3$ N/m	m_2	32 g
b	$0 - 50$ mm		
Reduced Parameters			
ε	0.76 %	λ_1	1.91
f_0	7.86 Hz		

Table 2. Simulation parameters for a cutting tool coupled with VI NES

Physical Parameters			
m_1	3.1 kg	μ_1	3 %
f_1	99.4 Hz	m_2	32 g
r	0.6		
Cutting Parameters			
p	0.1 mm	ρ_1	$6109.6 * 10^6$ Nm^{-2}
ρ_2	$-54141.6 * 10^9$ Nm^{-2}	ρ_3	$203.769 * 10^{12}$ Nm^{-2}
s	1800 rpm		

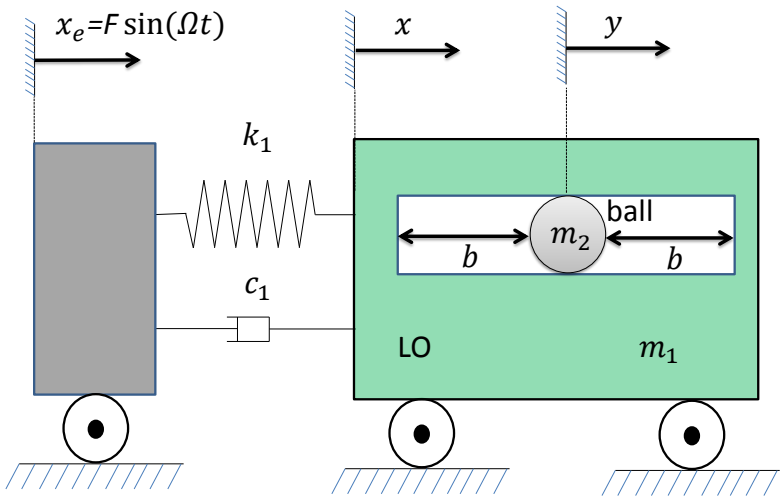

Fig. 1. Schema of a LO coupled with a VI NES under periodic excitation.

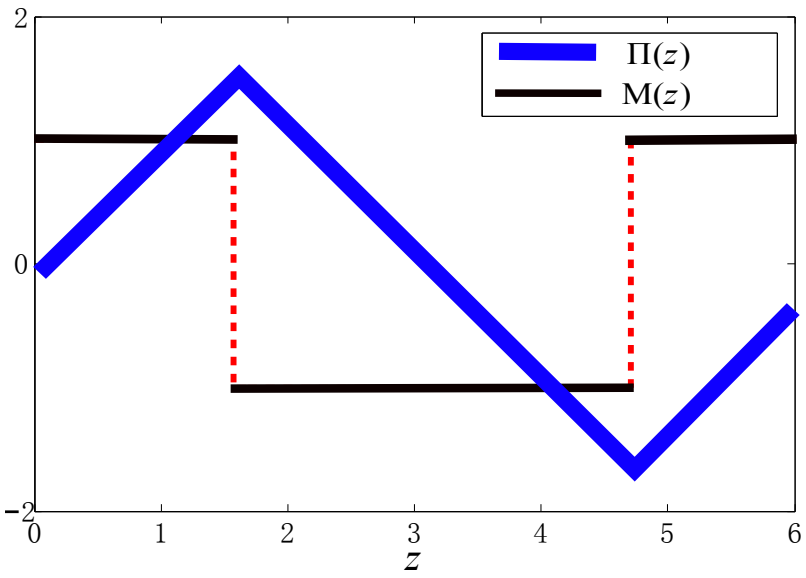

Fig. 2. Representation of the non-smooth functions $\Pi(z)$ in blue thick line and $\mathrm{M}(z)$ in black fine line and red dotted line.

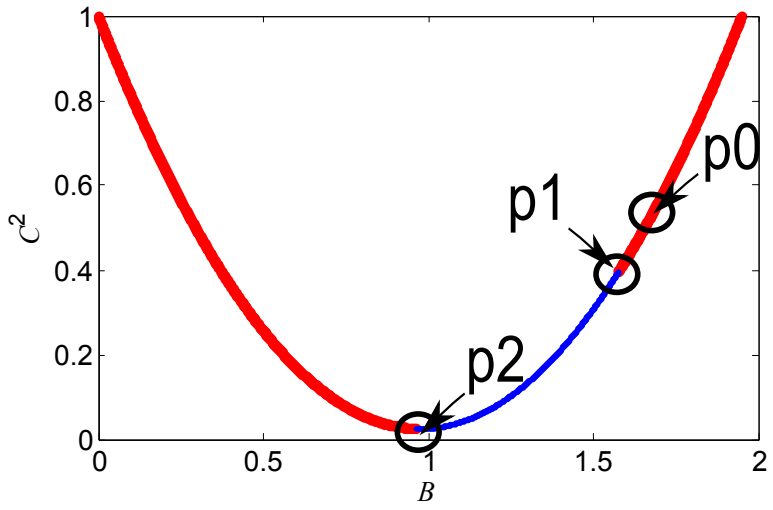

Fig. 3. SIM of VI NES: one stable branch in blue thin line and two unstable branches in red thick line with special points p0, p1 and p2.

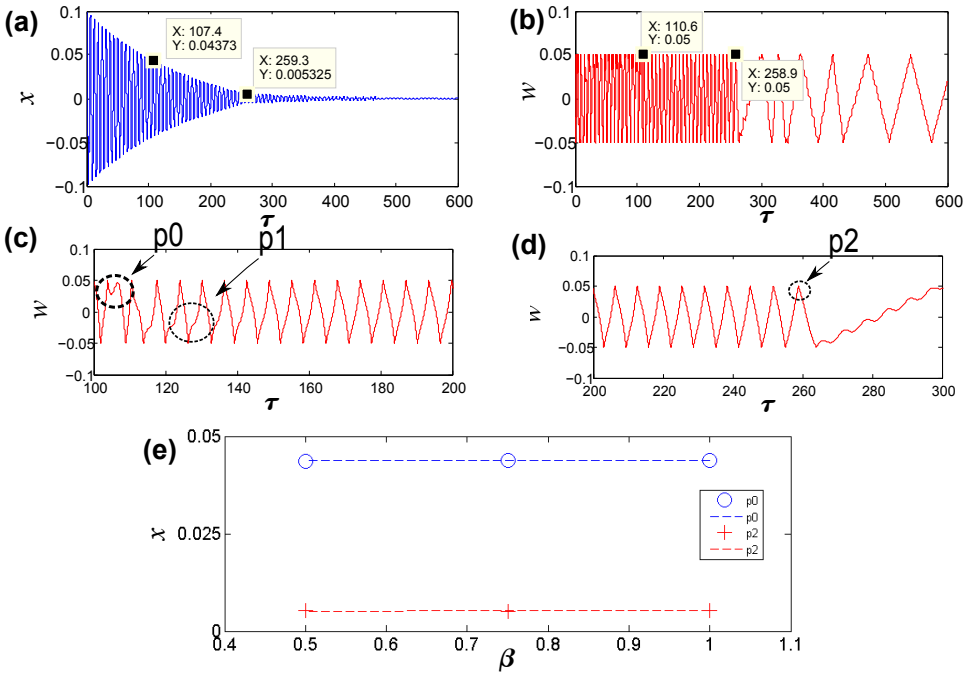

Fig. 4. Comparison of p0 and p2 for a LO with different natural frequencies: (a) the time history of displacement x; (b) the time history of relative displacement w; (c) the judge of p0 and p1 from w; (d) the judge of p2 from w; (e) x related to p0 and p2.

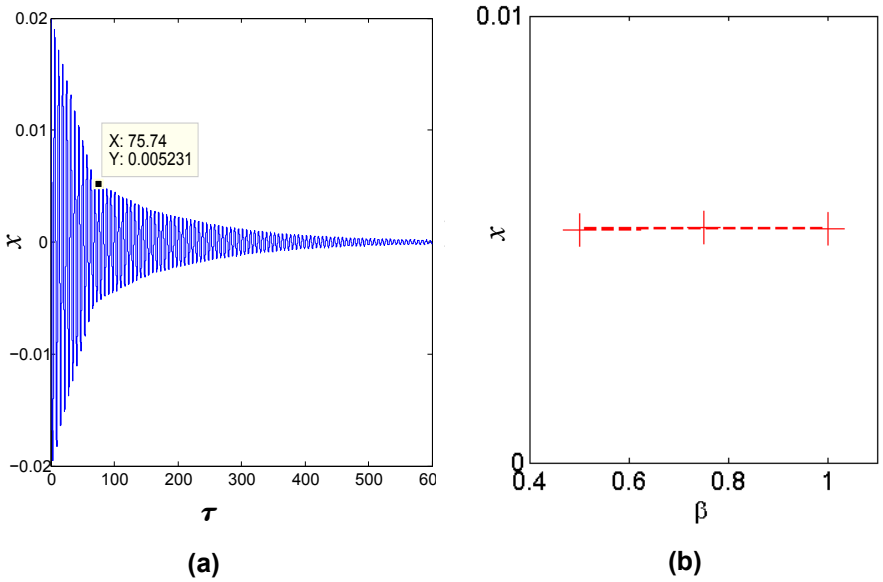

Fig. 5. Application of an optimal b from one specific LO to two other linear systems with different frequencies: (a) the time history of displacement of LO with $\beta = 1$; (b) x related to $p2$ for different β.

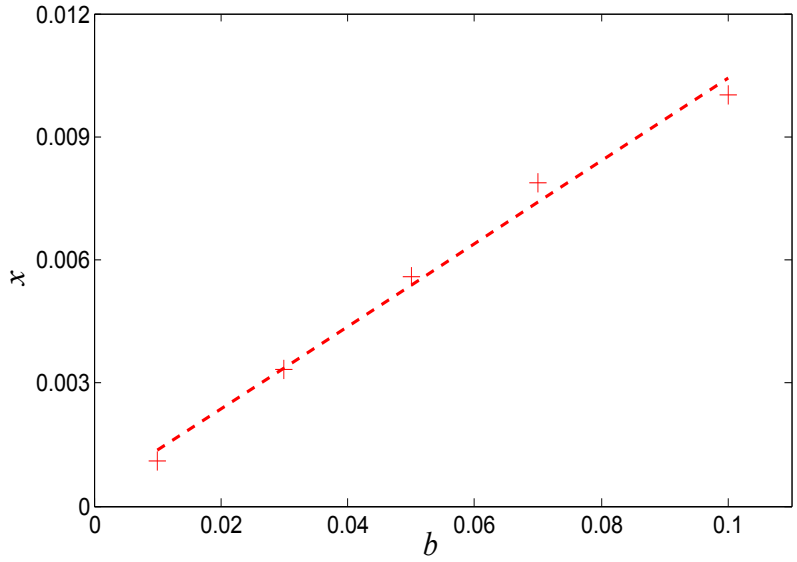

Fig. 6. x related to p2 and obtained from the response of a Duffing system with different b for VI NES.

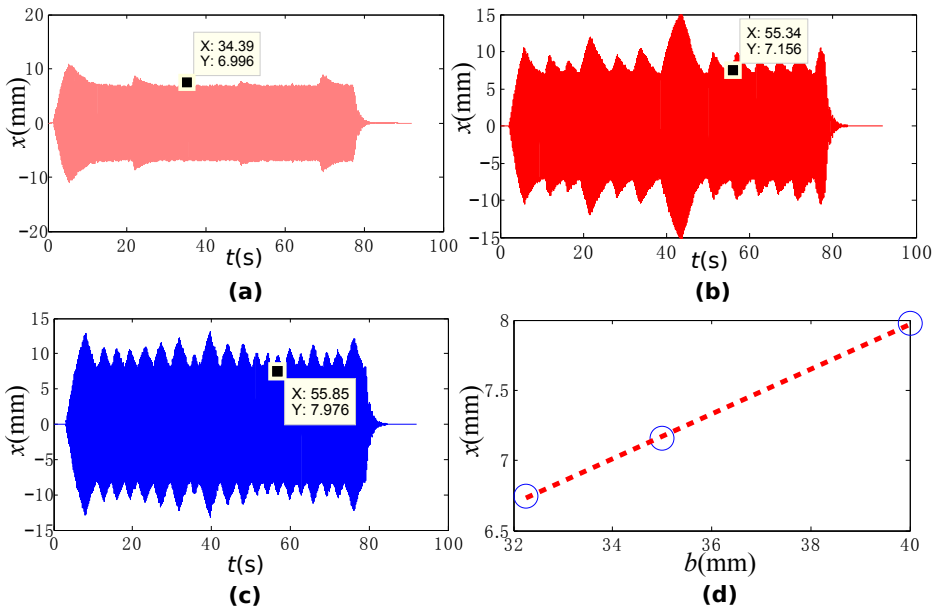

Fig. 7. Proportional activation characteristic of VI NES reflected by p2 of SIM: (a) $b = 32.5$ mm; (b) $b = 35$ mm; (c) $b = 40$ mm.

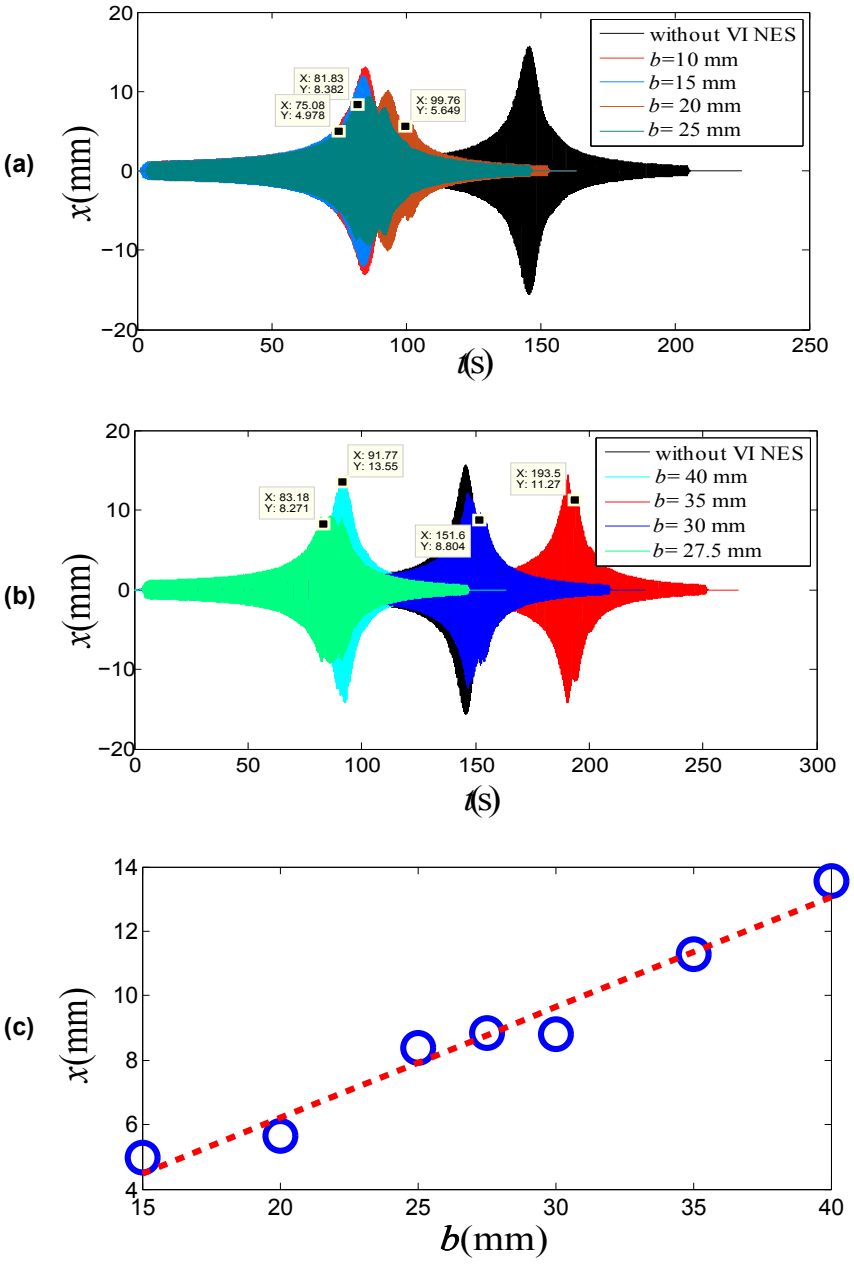

Fig. 8. Proportional activation characteristic of VI NES reflected by p2 of SIM from sweep experiment: (a) $b = 10$ mm, 15 mm, 20 mm and 25 mm; (b) $b = 27.5$ mm, 30 mm, 35 mm and 40 mm; (c) linear relation between b and x.

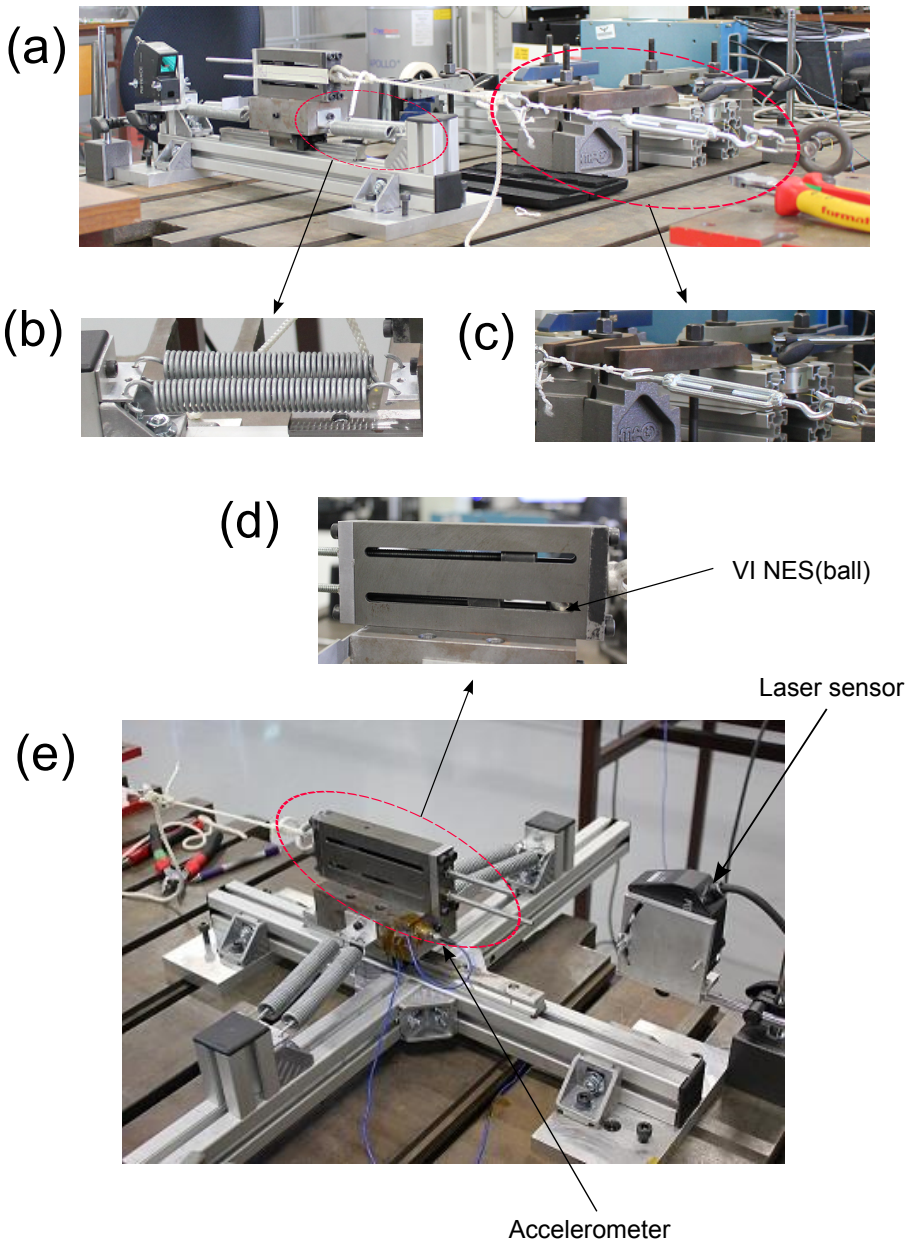

Fig. 9. Experimental setup: (a) linear systems with 4, 3 or 2 springs ; (b) the fixation of springs; (c) the regulation device of initial displacement; (d) an enlarged view of VI NES; (e) the Duffing system with 4 springs.

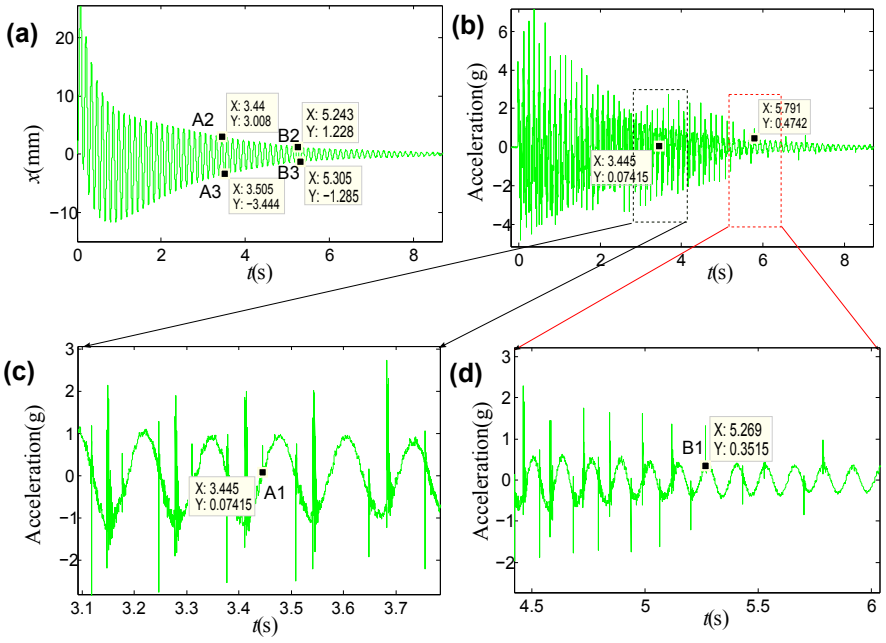

Fig. 10. LO with 4 springs and $b = 5$ mm: (a) the time history of displacement; (b) the time history of acceleration; (c) an enlarged view of the time history of acceleration around point A1; (d) an enlarged view of the time history of acceleration around point B1.

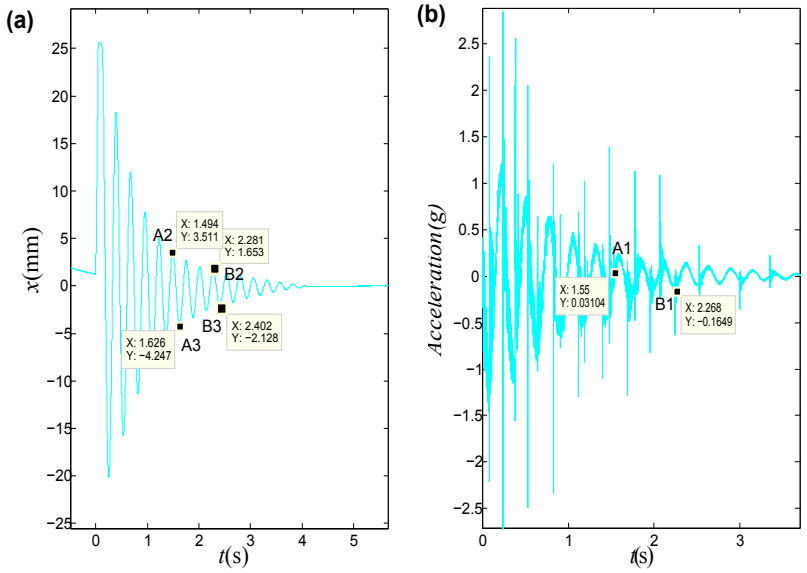

Fig. 11. Duffing system with 4 springs and $b = 5$ mm: (a) the time history of displacement; (b) the time history of acceleration.

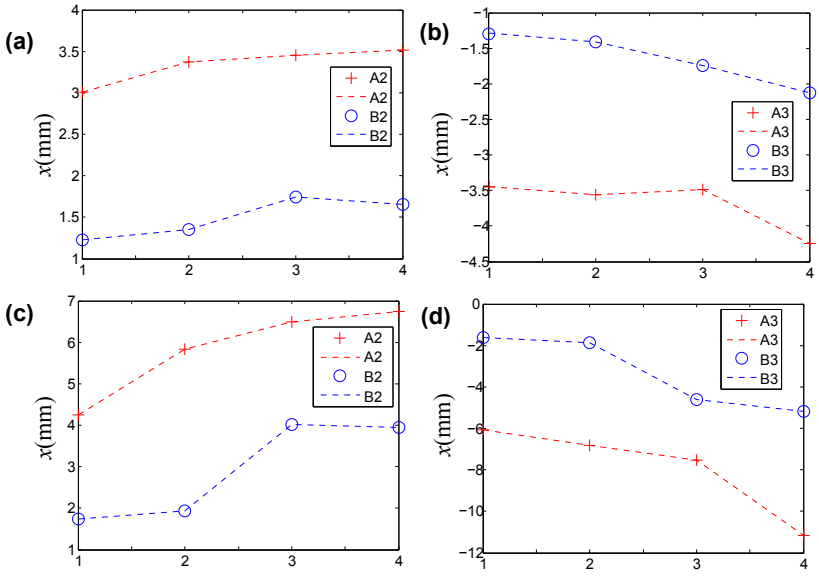

Fig. 12. Amplitude of the main structure around points A2, A3, B2 and B3 for three linear systems with 4, 3 and 2 springs and a Duffing system with four springs and these four systems are presented by 1,2,3 and 4 in the horizontal axis, respectively: (a) A2 and B2 with $b = 5$ mm; (b) A3 and B3 with $b = 5$ mm; (c) A2 and B2 with $b = 10$ mm; (d) A3 and B3 with $b = 10$ mm.

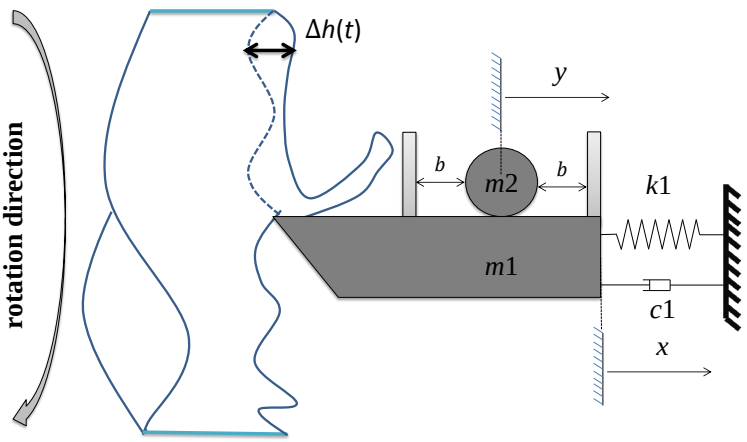

Fig. 13. Schema of a cutting tool system coupled with a VI NES.

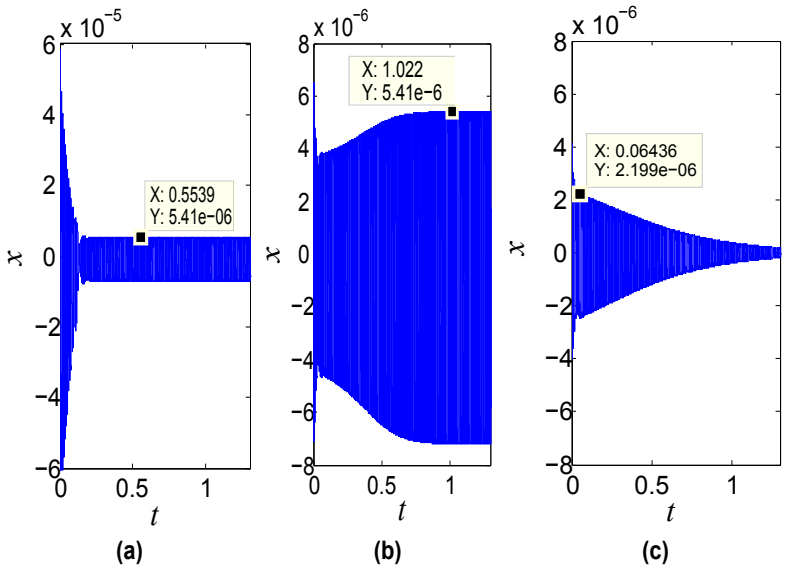

Fig. 14. Displacement of the cutting tool with different initial conditions for $h_0 = 0.11$ mm without VI NES: (a) $x_0 = 0.20$ mm; (b) $x_0 = 0.01$ mm; (c) $x_0 = 0.006$ mm.

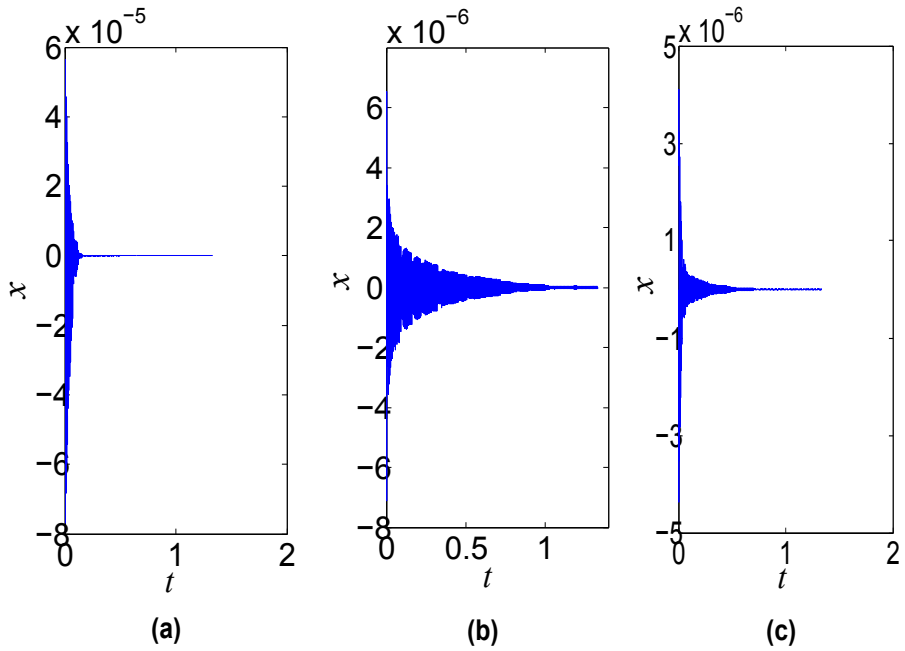

Fig. 15. Displacement of the cutting tool coupled with an effective VI NES for different initial conditions at $h_0 = 0.11$ mm: (a) $x_0 = 0.20$ mm and $b = 2.2880 * 10^{-2}$ mm; (b) $x_0 = 0.01$ mm and and $b = 2.2880 * 10^{-2}$ mm; (c) $x_0 = 0.006$ mm and $b = 2.4604 * 10^{-3}$ mm.

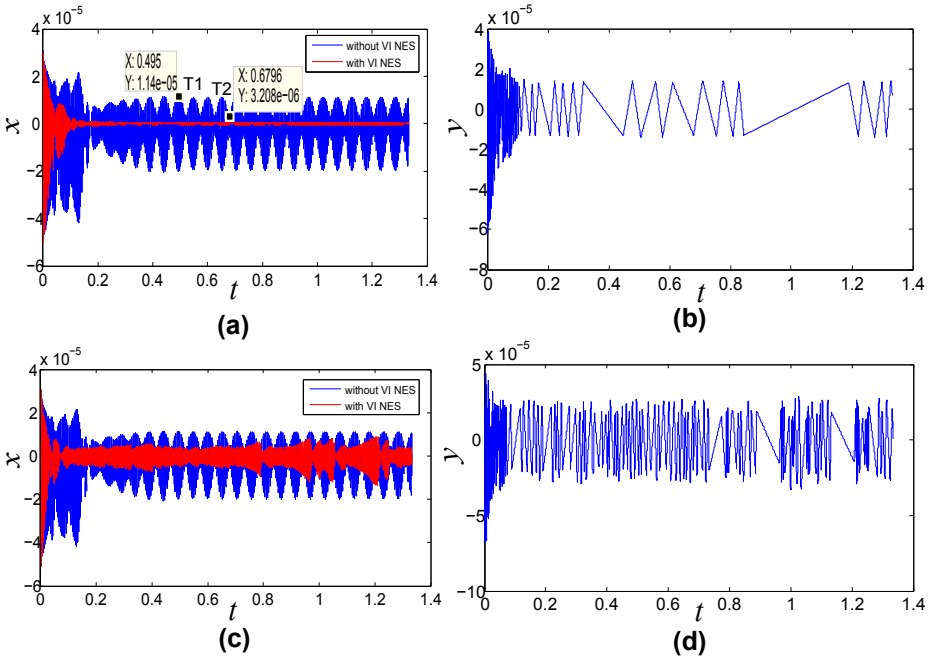

Fig. 16. Response comparison of the cutting tool without and with VI NES for $x_0 = 0.08$ mm and $h_0 = 0.16$ mm: (a) x and $b = 1.3517 * 10^{-2}$ mm; (b) y and $b = 1.3517 * 10^{-2}$ mm; (c) x and $b = 1.2632 * 10^{-2}$ mm; (d) y and $b = 1.2632 * 10^{-2}$ mm.

***Style Checklist**

Journal of Sound and Vibration

Author Checklist

Authors should complete the following checklist and submit with their revised manuscript.

Math notation follows requirements on Guide for Authors (GFA) see: ☑

https://www.elsevier.com/journals/journal-of-sound-and-vibration/0022-460X/guide-for-authors

Use Roman (normal upright) type for: Total differential operators (e.g. d in differential); i or j (square root of -1); exp or e (base of natural logarithms); Re or Im (real or imaginary part); log, ln, sin, cos, etc.; abbreviations such as c.c. (complex conjugate); multiletter symbols (e.g. TL for transmission loss); subscripts of two or more letters identifiable as words or word-abbreviations (e.g., Apipe, fmax) ☑

For more unusual functions, JSV follows Abramowitz and Stegun's book. More detail given in the GFA (see link above).

Unit symbols - These should be upright (e.g. kg, not *kg*). ☑

All authors are listed on the manuscript with correct affiliations, correct email address and are in correct order. ☑

Keywords present. ☑

Manuscript is not currently submitted to any other Journal. ☑

If submitting highlights please note that only six may be submitted and each one should be no longer than 85 characters in length. ☑

Novelty of paper has been clearly stated in the Introduction. ☑

References are presented as per GFA. ☑

References not produced in English language to have English translation in brackets. ☑

Figures and Tables and Equations are numbered in sequence correctly. (See GFA). ☑

Nomenclature (if required) appears on second page of submission. ☑

Acknowledgements appear in a separate section after the conclusion section but before references. ☑

All abbreviations, in both the abstract and main body of document, are defined once only, the first time they appear in the text. (N.B. The Abstract is treated as an independent text, where references are given in full and abbreviations and symbols, if used, are properly defined.) ☑

Figures – if there are multi-parts to a figures each part is labelled (a) (b) (c) etc. and the labels defined in the figure caption. ☑

Figures – Colour can be used for the on-line version. Figures are reproduced in black and white in the printed journal and must therefore be readable in both colour and black & white. (N.B. charges apply for production of colour figures in the printed journal) ☑

Appendices – should appear before the list of references and labelled A, B, C, (please see GFA for further information regarding equations, figures and tables in the appendices. ☑

Copyright – material reproduced from other publications (e.g. Tables, Figures), source is acknowledged. ☑

Statement of Author contribution complete (see GFA) ☑